Neptune Revisited: Synthesizing Coherent Doppler From Voyager's Noncoherent Downlink

T. A. Rebold, M. Tinto, and S. W. Asmar
Communications Systems and Research Section

E. R. Kursinski
Tracking Systems and Applications Section

In August 1989, Voyager 2 flew by the planet Neptune. Due to a faulty tracking-loop capacitor in the spacecraft's transponder, the last 25 minutes before ingress—the most critical period for obtaining coherent Doppler for gravity field analysis—had to be performed with the spacecraft assigned to the less-frequency-stable (but more reliable) noncoherent mode. The noncoherent downlink reduced the accuracy of the higher-order (J2 and J4) gravity terms [1]. However, a weak side tone, generated by the coherent oscillator feeding across the transponder mode switch, offered the possibility of extracting a coherent downlink from the noncoherent data. This article presents the results of synthesizing coherent Doppler from the Voyager feedthrough side tone. Furthermore, it shows how to form a linear combination of the two Doppler data sets that displays a lower noise level (30 to 50 percent at time scales of 300 seconds and above) for measuring the gravity field of Neptune.

I. Introduction

One of the primary missions of the Radio Science Systems Group at JPL is the performance of celestial mechanics experiments designed to measure fundamental gravity field parameters of the planets and moons encountered by spacecraft during flybys. Such quantities as mass, pole orientation, and gravity harmonics reveal much about the composition and internal structure of a celestial body that cannot be obtained any other way. Recent data from Galileo's tour of the Jovian system, for example, were used to infer working models of the interiors of Europa, Io, and Ganymede (including ferrous cores and the thickness of ice layers and oceans). These are just a few examples of what can be accomplished by gravity field measurements using spacecraft Doppler tracking [2].

A key factor in the success of these experiments is the frequency stability of the communication link to the spacecraft, since it is the small fluctuations in received Doppler frequency due to variations in the tug of gravity that form the basis of the measurements. Typically, spacecraft onboard ultrastable oscillators (USOs), with long-term stability of only 1 part in 10^{-12} or so,[1] are poor performers in this area compared with hydrogen masers on the ground. Because it is difficult to package the best frequency standards for space travel, a satisfactory solution is obtained with a transponder that locks to the uplink

[1] For Voyager-era USOs; current USOs can reach long-term stabilities of about 10^{-13}.

from Earth (generated by a hydrogen maser) and coherently transmits back to the ground. This coherent, or two-way, mode (three-way when the Earth receiving and transmitting stations differ) minimizes the spacecraft-generated frequency fluctuations in the radio link, making Doppler tracking a highly sensitive instrument for gravity field measurements.

In the case of Voyager 2, which began its tour of the outer planets in 1977, a failure in the transponder's phase-locked loop (PLL) capacitor while on its way to Jupiter left the spacecraft extremely sensitive to Doppler dynamics on the uplink, thus jeopardizing the link whenever coherent mode was selected. To prevent complete loss of telemetry data during critical encounters, Voyager was switched to noncoherent mode prior to the high Doppler dynamics of closest approach (even though the transponder remained locked to the uplink), thus sacrificing the most desirable data, from the standpoint of celestial mechanics researchers, at Saturn, Uranus, and Neptune.

With these considerations in mind, Kursinski proposed a solution that could partially restore the quality of Voyager's flyby data by taking advantage of a "flaw" in the transponder that allows coherent energy to leak onto the noncoherent downlink as a side tone appearing 27-dB below and 12.3-kHz away from the downlink carrier.[2] The process would be elaborate, requiring special software to detect the side tone phase, construct an effective coherent downlink time series, optimally combine the coherent and noncoherent data sets, and finally redo the gravity fit—all the while working with old, hastily archived data on new, sometimes incompatible computer systems. Furthermore, the whole endeavor could prove futile if the leakage process responsible for generating the side tone had any thermal instability associated with it.

Nonetheless, exploratory analysis by Kursinski[3] and Campbell[4] revealed that the potential reduction in Doppler noise could improve the accuracy of the Neptune gravity field measurement by up to 50 percent for selected gravity harmonics, and the development of a new technique for enhancing noncoherent Doppler could find many applications in fulfilling the competing interests of the space science community. This article documents the techniques of extracting and utilizing synthesized coherent Doppler—from theoretical prediction to application at Neptune. Section II presents a theoretical overview of side tone generation within the Voyager transponder, predicted improvement in Doppler frequency stability, and how the improvement can benefit gravity field measurements. Section III describes the processing steps using actual Voyager–Neptune data, including side tone detection, coherent downlink synthesis, and a new technique for optimally combining two data sets with different noise characteristics. Section IV evaluates the improvement exhibited in the final results, while Section V presents the conclusions along with several examples of current and planned missions that could benefit from the techniques outlined here.

II. Theoretical Background

A. Voyager Transponder

The mechanism that produces the coherent side tone can be seen in the spacecraft transponder diagram of Fig. 1. Through an elaborate system of frequency multipliers and mixers, a 19-MHz voltage-controlled oscillator (VCO) is phase locked to the incoming 2.3-GHz (S-band) uplink. In noncoherent mode, a switch in the transponder bypasses the VCO in favor of the onboard USO, a quartz crystal oscillator also tuned

[2] E. R. Kursinski, "A Proposal for a Simultaneous Coherent and Noncoherent Voyager Downlink Carrier Mode," JPL Interoffice Memorandum ERK-87-16 (internal document), Jet Propulsion Laboratory, Pasadena, California, May 6, 1987.

[3] E. R. Kursinski, "Combining USO and VCO Feedthrough Data," JPL Interoffice Memorandum ERK-87-17 (internal document), Jet Propulsion Laboratory, Pasadena, California, May 14, 1987.

[4] J. K. Campbell, "Potential Improvement in Neptune Gravity Parameter Determination With Synthesized Coherent Data," JPL Interoffice Memorandum MGN-NAV-89-126 (internal document), Jet Propulsion Laboratory, Pasadena, California, October 5, 1989.

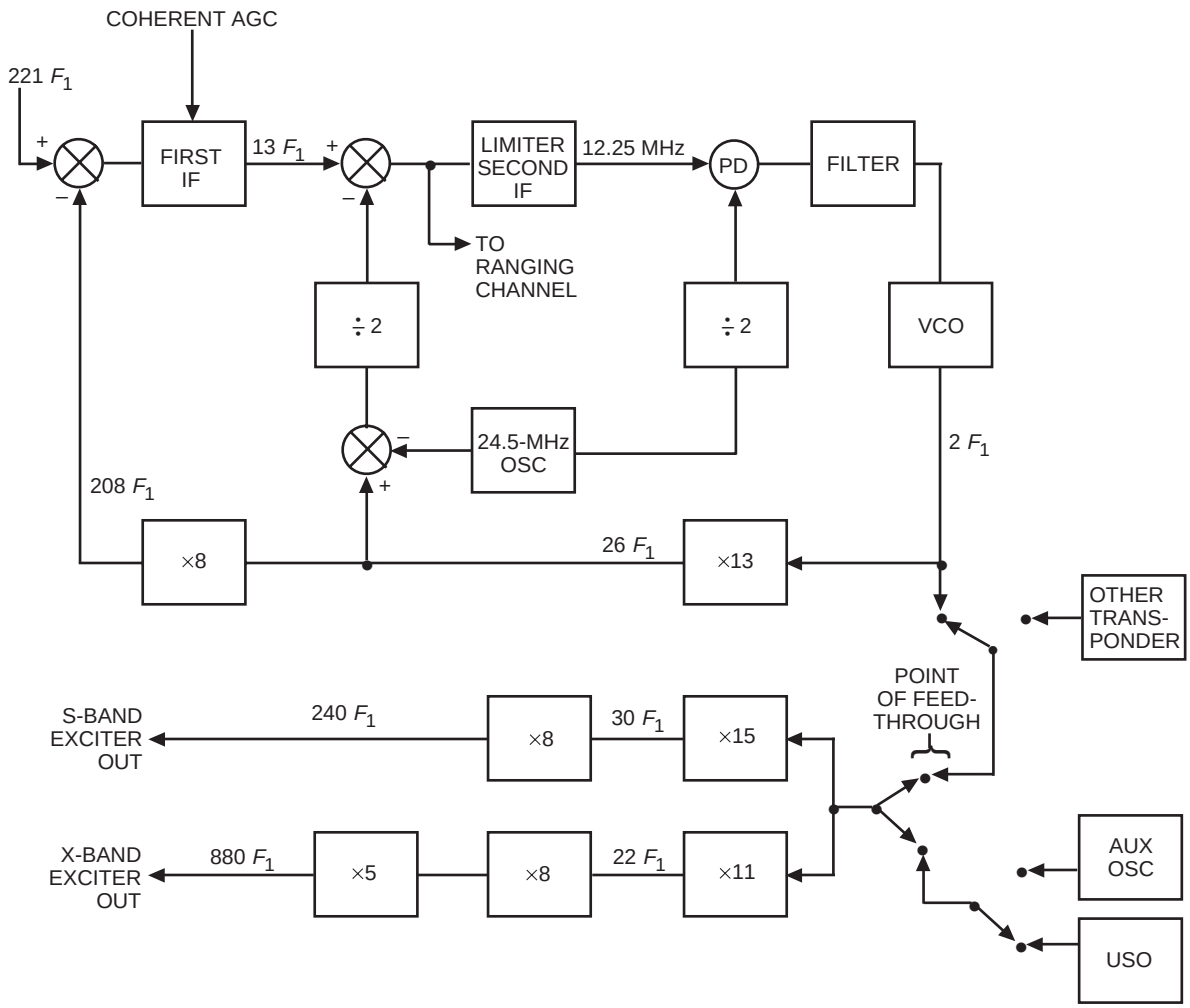

Fig. 1. Voyager receiver–exciter functional block diagram, showing the transponder mode switch, the point of VCO feedthrough onto the USO downlink (where AGC is the active gain control, PD is the phase detector, and AUX OSC is the auxiliary oscillator).

to 19 MHz. However, imperfections in the transponder mode switch (designed with 80 dB of isolation) allow a small but significant amount of VCO signal to pass, forming a spurious tone 80-dB below and 12.3-kHz away (the difference frequency at 19 MHz) from the USO carrier.

Mathematically, the combined signal $S(t)$ at the output of the switch can be described by

$$S(t) = A_{u19} \cos\left[2\pi f_{u19} t + B \sin\left(2\pi f_m t + \phi_{19}\right)\right] \tag{1}$$

where A_{u19} and f_{u19} are the USO amplitude and frequency at 19 MHz, $B = \sqrt{G_i} = 1/10,000$, G_i is the isolation across the switch, f_m is the difference frequency between the USO and VCO at 19 MHz (about 12.3 kHz), and ϕ_{19} is the modulation phase at $t = 0$. In this form, the signal can be regarded as a 19-MHz USO with a single-tone phase modulation at the difference frequency between the two oscillators.

If the side tone remained at −80 dBc, there would be no possibility of recovering it; however, in frequency multiplying the output of the switch by 440 to 8.4 GHz (X-band), the side tone gets amplified by 53 dB ($20 \log_{10}(440)$), bringing it to a level of −27 dBc:

$$S_x(t) = A_x \cos\left(2\pi f_{ux} t + 440B \sin(2\pi f_m t + \phi_{19})\right) \tag{2}$$

where $f_{ux} = 440 f_{u19}$, the transmitted noncoherent frequency. Note that because the frequency multiplication does not affect the side tone frequency (only the amplitude), it remains 12.3-kHz away from the carrier even at X-band.

Incidentally, the 12.3-kHz separation is not arbitrary. The presence of a side tone close to the carrier at −27 dBc could seriously degrade the stability and spectral purity of the X-band downlink, affecting radio science as well as navigation and telemetry performance. Consequently, the designers of the Voyager transponder intentionally separated the USO and VCO frequencies (at the 19-MHz level) by that amount (a distance of four Deep Space Network (DSN) channels), leading to a relatively large separation of 5.4 MHz at X-band between the coherent and noncoherent downlink channels.

Neglecting for simplicity the effect of Doppler shift, recovery of a coherent downlink from the received noncoherent downlink can now proceed by (1) tracking $f_{ux}(t)$, the noncoherent downlink frequency, (2) tracking $f_m(t)$, the 12.3-kHz side tone frequency, and (3) computing the coherent downlink frequency:

$$f_{vx}(t) = f_{ux}(t) - 440 f_m(t) \tag{3}$$

where f_{vx} is the frequency of the VCO multiplied by 440.

There are two limits to the frequency stability of this synthesized coherent downlink: (1) the weak signal-to-noise ratio (SNR) of the side tone (27-dB weaker than the USO downlink), which corrupts the short-term stability (1 to 100 seconds) and (2) the need to multiply the side tone frequency by 440 after receiving it on the ground, which makes the thermal noise 440 times more significant (in a $\Delta f/F$ sense) than that for a normal 8.4-GHz coherent downlink.

B. Improvement in Doppler Frequency Stability

Ultimately, the purpose of extracting a coherent downlink from noncoherent data is to improve upon the long-term (greater than 100-s) frequency stability of the noncoherent USO. Because of its poor short-term stability, the synthesized VCO data must be combined with the USO in a manner that minimizes the total frequency noise without distorting the underlying Doppler signature. To accomplish this, Kursinski proposed a Fourier technique that would select components below a certain cutoff frequency from the VCO data and above the cutoff from the USO data.[5] If done properly, this would result in a new data set with the short-term stability of the USO and the long-term stability of the VCO.

Unfortunately, the two data sets could not be combined directly because coherent and noncoherent frequency data do not measure the same velocities. Coherent data measure Doppler due to Earth motion at Earth transmit time, spacecraft motion at spacecraft receive (and transmit) time, and Earth motion at Earth receive time. On the other hand, noncoherent data measure Doppler due to spacecraft motion at spacecraft transmit time and Earth motion at Earth receive time. In order to combine the two data sets, the effect of Earth Doppler must be removed, and the frequencies must be converted to units of velocity (since the noncoherent frequency data are approximately half as sensitive to velocity as are the coherent data):

$$S_v = \left(\frac{c}{2}\right)^2 S_y \tag{4}$$

for coherent data and

[5] E. R. Kursinski, May 14, 1987, op cit.

$$S_v = c^2 S_y \tag{5}$$

for noncoherent data, where S_v is the one-sided velocity power spectral density, c is the speed of light, S_y is the normalized frequency (f/F_0) power spectral density, and F_0 is the transmit frequency.

Figure 2 shows three curves demonstrating three limiting factors in the measurement of radial velocity with Doppler frequency data: plasma on the S-band uplink for coherent data, the instability of the USO for noncoherent data, and the combined effect of low SNR and low effective carrier frequency of the synthesized coherent VCO data (assuming a side tone level of −178 dBm). The thick line in the figure represents the noise level of an optimally combined coherent/noncoherent data set. Thus, even with the weak side tone SNR, the synthesized coherent data can improve upon the USO (by 10 dB or more) for time scales greater than 300 s (frequencies less than 3 mHz).

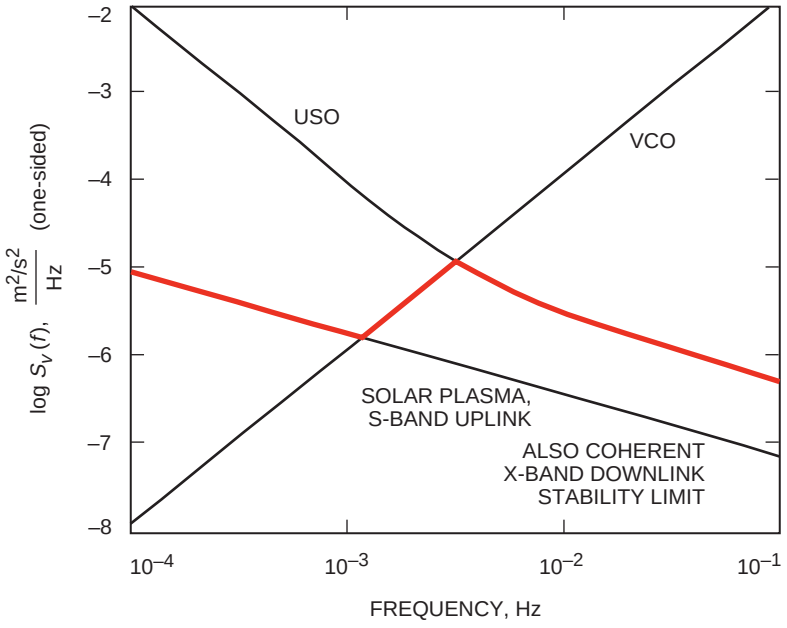

Fig. 2. Estimate of Doppler velocity measurement sensitivity (i.e., noise floor) for three different noise sources: USO, synthesized VCO, and solar plasma on the S-band uplink (assuming a Sun–Earth–probe angle of 125 deg).

C. Application to Gravity Field Measurements

Every time a spacecraft flies past or around a body, it acts as a test mass for probing the local gravity field. By simply keeping track of the minute fluctuations in spacecraft velocity (or Doppler shift) as the spacecraft coasts in free-fall, scientists can derive not only a planet's mass but also the higher-order harmonics of its gravity field:

$$g(r,\varphi) = \frac{GM}{r^2}\left(1 + 3J_2\left(\frac{R}{r}\right)^2 P_2(\varphi) + 5J_4\left(\frac{R}{r}\right)^4 P_4(\varphi)\ldots\right) \tag{6}$$

where G is the universal gravitational constant, M is the mass of the planet, $J_{2,4}$ are the second and fourth zonal harmonic coefficients, R is the radius of the planet, and $P_{2,4}(\varphi)$ are the second- and fourth-order Legendre polynomials as a function of latitude, φ. From the higher J-coefficients, such things as mass concentrations, internal structure (solid versus gaseous cores), and shape (deviations from sphericity) can

be inferred. The actual derivation of the harmonic coefficients is performed by fitting a parameterized orbital model, including the planet's gravitational field, to the observed Doppler frequency time series by weighted non-linear least squares [3].

Although in principle there is no limit to the harmonic structure of a planet's gravity field (a lunar orbiter experiment derived the first 106 gravity harmonics for the Moon), at Neptune the single-pass flyby trajectory restricted the analysis to J4 and below, but was further degraded by lack of coherent data at closest approach. Shortly after the encounter, Campbell investigated the potential sensitivity to be gained from including the synthesized coherent data (at stabilities consistent with Kursinski's analysis) from three different periods of noncoherent data near closest approach.[6] His findings, summarized in Table 1, reveal that (1) only the 25-min region immediately prior to ingress (07:42:00 to 08:05:00 Earth received time) can provide significant additional information on the gravity field and (2) measurement uncertainty for harmonics J2 through J6 could be reduced by 25 to 60 percent with these data. A plot of the Doppler signatures for an arbitrary harmonic perturbation of 2×10^{-6} in J2, J4, and J6 (Fig. 3) shows why the middle region is most significant and illustrates the type of effect that should be observed in the final results.

Of particular interest to the space science community was the possibility of narrowing the uncertainty of J4 to the point where inferences could be made about the suspected solid core of Neptune. It was this possibility that motivated the following effort to actually extract the coherent downlink and see if, in this case, theory could effectively be put to practice.

Table 1. Neptune gravity harmonic parameters and uncertainties from the original gravity field estimate, with expected uncertainties using synthesized coherent Doppler from Neptune ingress.[a]

Parameter	Original estimate ($\times 10^{-6}$)	$\sigma(\times 10^{-6})$	Expected σ using synthesized coherent Doppler ($\times 10^{-6}$)
J2	3410.5	6.8	3.3
J3	0	7.9	4.7
J4	−34.7	9.4	5.9
J5	0	7.4	5.3
J6	0	7.9	2.5

[a] From J. K. Campbell, op cit.

III. Signal Processing

The analysis begins with a set of 9-mm tapes recorded at the Parkes 64-m radio telescope in Australia during the Neptune flyby. The tapes contain approximately 35 kHz of X-band spectrum sampled at 80 ksamples/s (kS/s), recorded in typical radio science open-loop fashion using an old occultation data assembly (ODA). The ODA was installed temporarily at Parkes, along with an X-band downconverter, to permit signal arraying with the DSN 70-m antenna at Canberra during the crucial minutes of the flyby [4,5]. A programmable oscillator control assembly (POCA) was used to freeze the signal within the sample band using a series of fixed ramp rates. Although X-band data from both Canberra and

[6] J. K. Campbell, op cit.

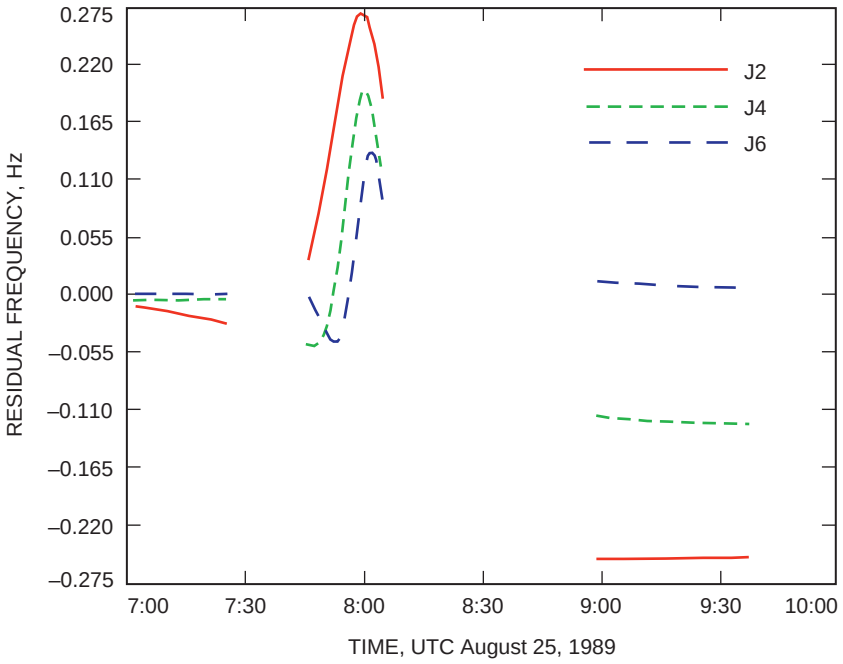

Fig. 3. The Doppler velocity signatures for the J2, J4, and J6 gravity harmonics during three nonconcoherent tracking periods at Neptune flyby.

Parkes were recorded, the Parkes data encompass the wider sample bandwidth (35 as opposed to 20 kHz) necessary to include both spurious side tones (±12.3 kHz) in the data set.

Figure 4 shows the power spectrum of the signal recorded on tape at Parkes, with both the carrier and the two side tones appearing in the 35-kHz filter bandwidth. The carrier SNR is approximately 42 dB-Hz. Although the side tones fall about 35-dB below the carrier (8-dB lower than Kursinski's estimate), due to a higher overall signal strength, the side tone power level is very close to the −178-dBm assumption illustrated in Fig. 2. The following sections trace the evolution of the recorded signal as it undergoes baseband detection, noncoherent and coherent sky frequency derivation, and optimal combining in the Fourier domain.

A. Baseband Detection

Figure 5 outlines the baseband detection procedure, essentially a software receiver that tracks both the USO carrier and the side tone. It utilizes a quadrature mixer (phase detector) on the carrier to consolidate the double-sided side tone spectrum into a single tone (representing the sum power of both side tones) that then can be detected in a single pass.

The success of this strategy hinges upon the phase detection algorithm, in this case a nonlinear least-squares fit routine based on the MRQMIN Marqhardt–Levenberg program [6], but referred to here as FITIQ because it has been adapted to work on complex in-phase and quadrature-phase (I&Q) signal representations. In practice, FITIQ performs much the same as a phase-locked loop (PLL) in that both measure signal frequency, amplitude, and phase. However, FITIQ benefits from a memoryless, responsive estimation (useful at POCA ramp changes) and the intuitive simplicity of the least-squares approach.

As shown in Fig. 5, the processing architecture contains several stages of filtering and decimation prior to FITIQ in order to (1) reduce the noise of the signal and (2) increase the processing speed of FITIQ. For the USO detection, the sample rate was reduced by 20 to 4000 samples/s (S/s), while for the side tone the reduction was a factor of 400 (200 S/s). Estimates of the strong 40-dB-Hz carrier were made

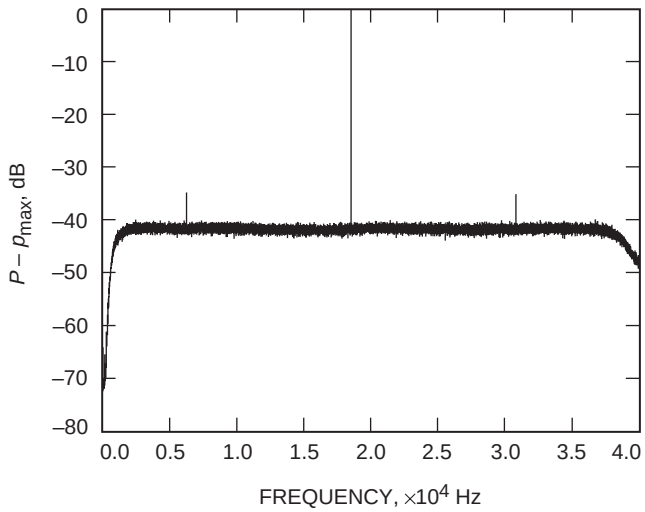

Fig. 4. The fast Fourier transform of the recorded USO downlink from Parkes, Australia, showing an approximate 42-dB-Hz carrier SNR and 6- to 7-dB-Hz side tones from the VCO feedthrough effect.

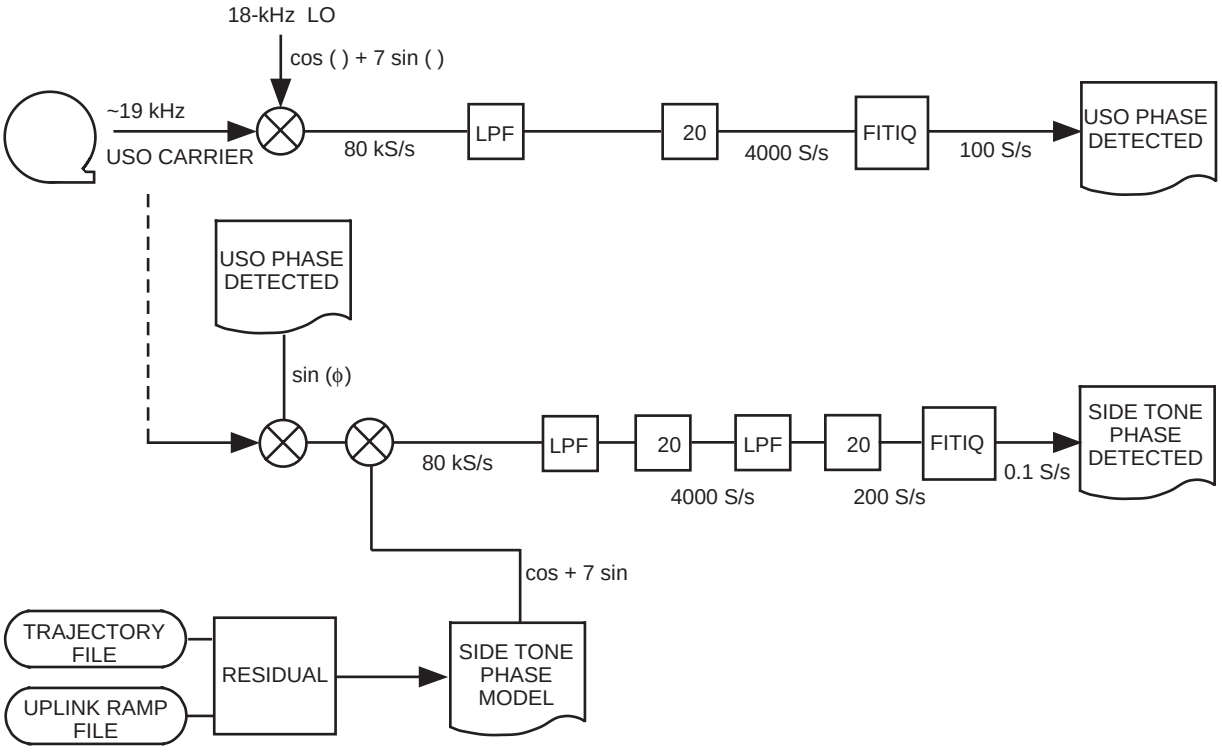

Fig. 5. The signal detection architecture. Above is the USO phase detection, and below is the side tone phase detection using results of the USO detection and side tone phase model from the trajectory and uplink predicts (where LPF denotes the low-pass filter).

over 0.01 s to track the abrupt frequency cusps at POCA ramp changes, while estimates of the weak 9-dB-Hz side tone were performed over 10 s to average out the thermal noise.

Two signal phase models are required in the reduction of side tone data: one for the USO phase, necessary for the quadrature mixer, and the other for the side tone phase, necessary to remove the effect

of uplink POCA ramp changes on the 10-s side tone detection. Whereas the first model follows directly from the USO detection, the second model is not so easily derived. It requires modifying the program RESIDUAL (a radio science utility that removes the expected Doppler, based on a given spacecraft trajectory, from a set of observed sky frequencies) to produce a time series of one-way Doppler scale factors, $D(t)$, and predicted VCO frequencies, $f_{v19}(t)$, based on the uplink frequency received at the spacecraft. Once these quantities are obtained, the side tone phase model is derived by integrating the following:

$$f_m(t) = D(t)\,(f_{u19} - f_{v19}(t)) \tag{7}$$

where $D(t) = (1 - v(t)/c)$ (plus higher-order terms [8]), the one-way Doppler scale factor based on spacecraft velocity and the speed of light, and f_{u19} is the fixed USO frequency at 19 MHz

Figure 6 shows the detected USO carrier frequency at baseband, complete with tuning scallops from the POCA ramp changes, that was integrated to form the USO phase model. Figure 7 shows the side tone frequency model generated from RESIDUAL, with a similar set of scallops from the uplink tuning, that was removed prior to detecting the side tone. Finally, Fig. 8 shows the detected side tone frequencies. To arrive at the actual side tone "sky" frequencies, the frequency time series in Fig. 8 must be added to that of Fig. 7.

B. Coherent Sky Frequency and Doppler Residuals

Following baseband detection, a set of sky frequencies (Doppler-shifted spacecraft transmit frequency as seen by the Earth receiving antenna) was generated for the noncoherent data using

$$f_{u_{\rm sky}}(t) = f_{u_{bb}}(t) + 7f_{\rm POCA}(t) + f_{LO} \tag{8}$$

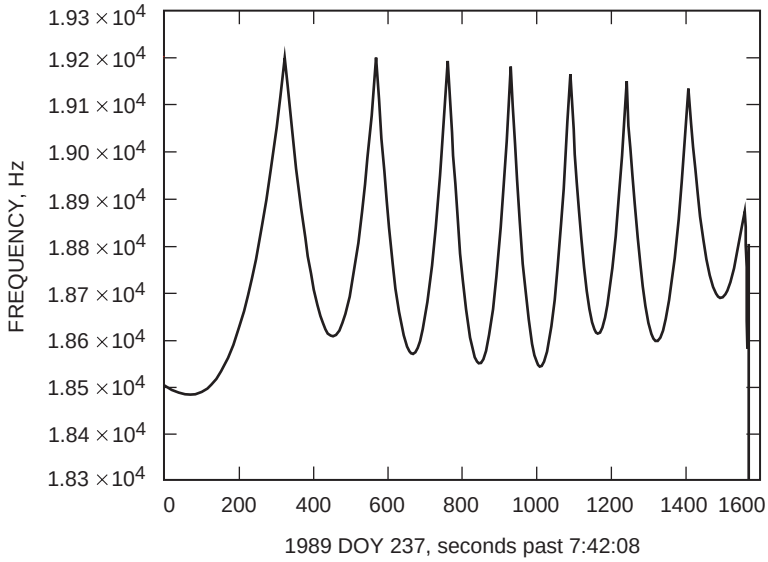

Fig. 6. The detected USO downlink frequency as recorded at Parkes, showing tuning scallops from the receiver programmable oscillator (i.e., linear ramp removal).

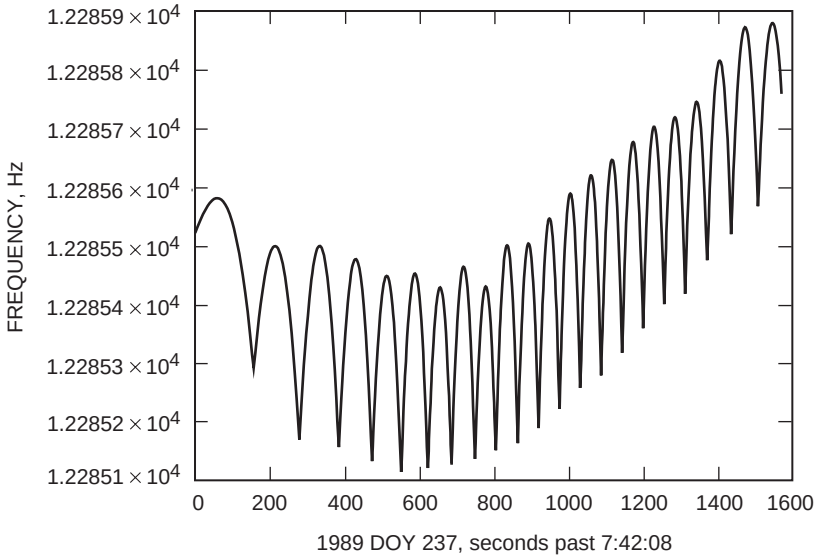

Fig. 7. The predicted side tone frequency based on uplink tuning, flyby trajectory predicts, and one-way Doppler shift.

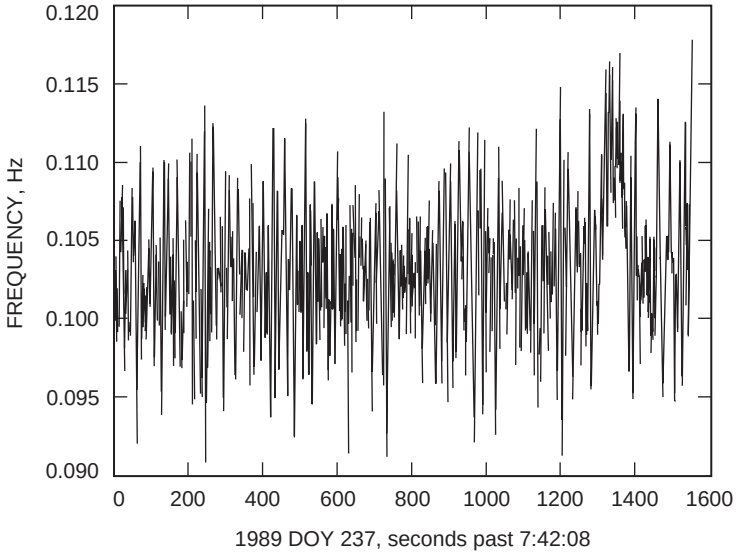

Fig. 8. The detected side tone frequency after removal of the prediction.

where $f_{u_{bb}}(t)$ is the detected noncoherent baseband frequency, $f_{\mathrm{POCA}}(t)$ is the POCA programmable oscillator frequency, and f_{LO} is the fixed receiver's first local oscillator frequency, 8.1 GHz. This equation is specific to the Parkes implementation.

For coherent data, obtaining sky frequency estimates is simply a matter of shifting the one-way sky frequencies by 440 times the side tone frequency (the difference between the two oscillators on board the spacecraft at 19 MHz). The effect of Doppler shift, neglected in Eq. (3), is not significant, since it applies equally to both USO and side tone frequencies. What is detected on the ground are the Doppler-shifted USO and side tone, i.e.,

$$f_{u_{\rm sky}}(t) = D(t) f_{ux} \tag{9}$$

$$f_{m_{\rm sky}}(t) = D(t) f_m(t) = D(t)(f_{u19} - f_{v19}(t)) \tag{10}$$

where f_{ux} is the fixed USO transmit frequency; $f_m(t)$ is the side tone transmit frequency, $f_{u19} - f_{v19}(t)$; and $D(t)$ is the one-way Doppler scale factor.

Note that the uplink Doppler and uplink transmit frequency are already incorporated into $F_{v19}(t)$, the onboard VCO frequency locked to the uplink. When Eq. (3) is applied to generate coherent data, what results is

$$\begin{aligned} f_{v_{\rm sky}}(t) &= f_{u_{\rm sky}}(t) - 440 f_{m_{\rm sky}}(t) \\ &= D(t) \times f_{ux} - 440 D(t) f_m(t) \\ &= 440 D(t) f_{u19} - 440 D(t) f_{u19} + 440 D(t) f_{v19}(t) \\ &= D(t) f_{vx}(t) \end{aligned} \tag{11}$$

where $f_{m_{\rm sky}}$ is the detected side tone frequency.

In practice, extreme care must be exercised to line up the time tags between the two data streams, each of which undergoes a different time delay from using different estimation strategies. This was accomplished by picking a convenient offset into the dense 0.01-s USO estimates before averaging to 1 s, and by discarding the first reduced side tone sample (a shift of 0.05 s) before starting FITIQ. The final noncoherent sky frequencies have an estimation period of 1 s, while the synthesized coherent sky frequencies, though sampled every second (at the same time as the noncoherent data), have an estimation period of 10 s.

Figure 9 shows what must be one of the first instances of simultaneous coherent and noncoherent sky frequencies obtained from a deep-space probe. Prior to being occulted by the Neptune atmosphere, the spacecraft experienced a sudden deceleration as it reached the far side of the gravity well, generating the U-shaped sky frequency signature shown in the plots. Both noncoherent and coherent data have very similar shapes because the uplink from Earth was tuned to remain stationary (to within 80 Hz) at the spacecraft. The actual differences between the two data sets cannot be observed until the dominating Doppler shift has been removed.

Thanks to the archiving efforts of several people on the navigation team, the post-fit Voyager–Neptune trajectory from 1989 [7] was still available for processing these recently generated data sets. Doppler, uplink tuning, and first-order gravitation effects (including gravity field and gravitational redshift) were removed from the data, resulting in the residual frequencies (both coherent and noncoherent) shown in Fig. 10. In this figure, the short-term noise of the coherent Doppler residuals easily exceeds that of the noncoherent residuals by a factor of 100, as is expected from the much weaker SNR of the side tone. Also, one can observe the long-term $1/f$ drift in the noncoherent data that masks the higher-order gravity field harmonics. The question that remains to be answered is if, buried within the noise, the coherent data have any new information on the gravity field of Neptune.

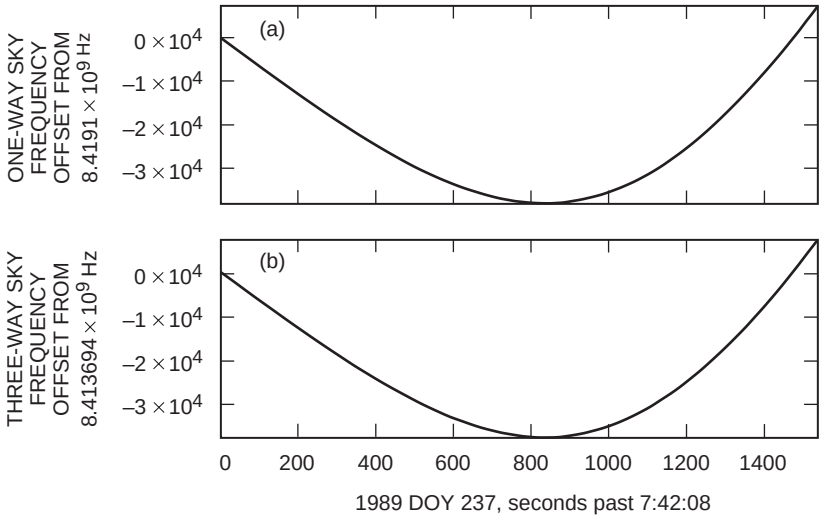

Fig. 9. The sky frequencies appearing at the input to the Parkes antenna: (a) noncoherent and (b) synthesized coherent.

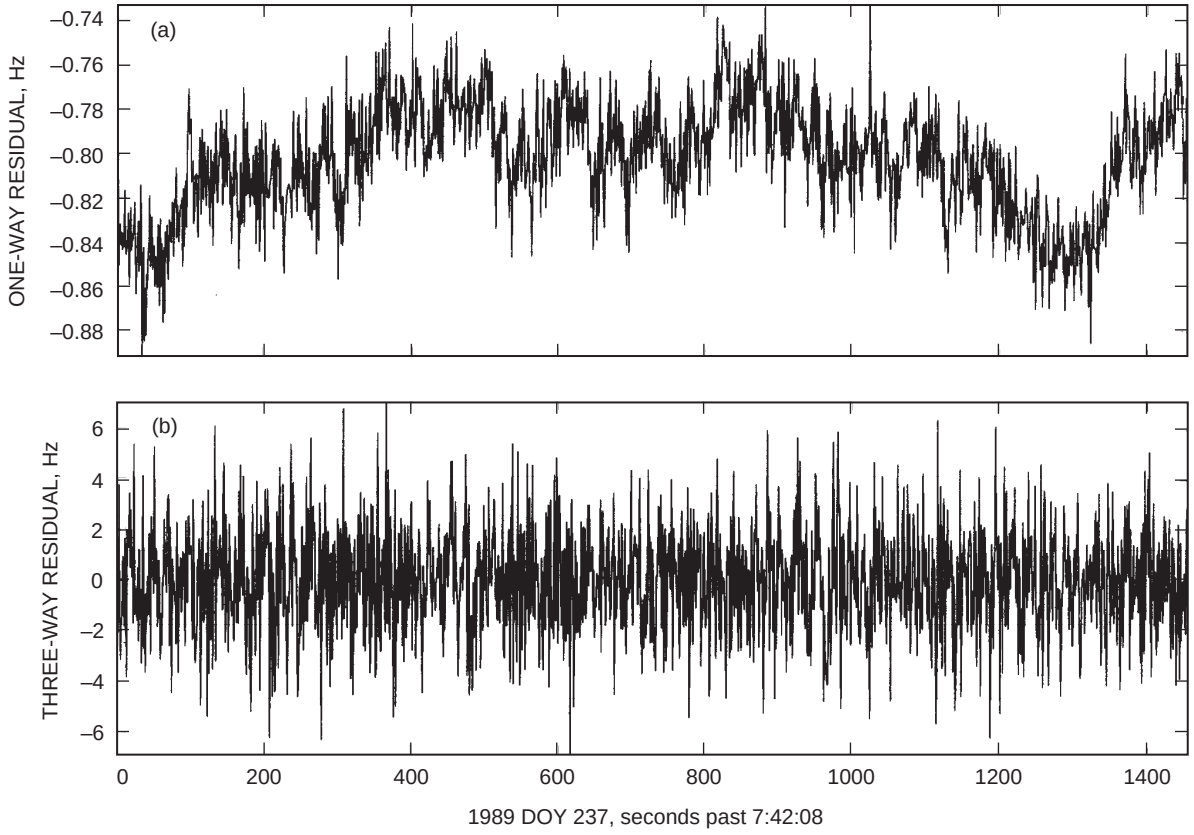

Fig. 10. The residual frequency after removal of the 1990 trajectory solution: (a) noncoherent and (b) synthesized coherent.

C. Optimal Combining

At this point, two versions of spacecraft Doppler, with two different frequency noise characteristics, have been produced: a noncoherent set that follows the $1/f$ "flicker frequency" noise power distribution of the USO (i.e., noisier at low frequencies) and a synthesized coherent set that displays an $f2$ frequency noise distribution (i.e., noisier at high frequencies) due to the white phase noise of the weak side tone SNR. A separate study by Kursinski and Tinto developed the concept of Fourier combining the two data sets in a way that selects their least noisy components while retaining the integrity of the underlying gravity signature.[7] The idea is to Fourier transform both the coherent and noncoherent data sets; sum them together using a pair of weighting functions, $a(f)$ and $b(f)$; and inverse transform the sum back into the time domain. Mathematically, the combining operation can be described by

$$C(f) = a(f)V(f) + b(f)U(f) \tag{12}$$

where V and U are the Fourier transforms of the USO and VCO velocity time series, and a and b are the weighting functions, defined such that they minimize the noise summation at each frequency bin. Derivation of the weighting functions starts with breaking the two data sets into their noise and signal components:

$$V(f) = N_{\text{vco}}(f) + S(f) \tag{13}$$

$$U(f) = N_{\text{uso}}(f) + S(f) \tag{14}$$

where $S(f)$ is the Fourier transform of the gravity signature, $s(t)$, embedded in both data sets and $N_{\text{uso}}(f)$ and $N_{\text{vco}}(f)$ are the transforms of the respective noise processes. One can see that, to ensure that $S(f)$ remains unmodified in the final combination, $C(f)$, it becomes necessary to add the constraint

$$a(f) + b(f) = 1 \tag{15}$$

Substituting Eqs. (13), (14), and (15) into Eq. (12), we get

$$C(f) = S(f) + a(f)N_{\text{uso}}(f) + (1 - a(f))N_{\text{vco}}(f) \tag{16}$$

The combined data set, $C(f)$, has a signal and a noise component. Assuming that the two noise processes are uncorrelated, the total noise power in $C(f)$ can be written as

$$P_n(f) = a(f)^2 P_{\text{uso}}(f) + (1 - a(f))^2 P_{\text{vco}}(f) \tag{17}$$

where $P_{\text{uso}}(f)$ and $P_{\text{vco}}(f)$ are the noise power spectral densities of $N_{\text{uso}}(f)$ and $N_{\text{vco}}(f)$. The problem then becomes one of minimizing $P_n(f)$ for all frequencies. Taking the derivative of $P_n(f)$ with respect to $a(f)$ and setting it equal to zero, the following solution emerges:

---

[7] E. R. Kursinski and M. Tinto, "Optimal Weighting of the VCO and USO Data Sets in the Fourier Domain," JPL Interoffice Memorandum 3394-93-29 (internal document), Jet Propulsion Laboratory, Pasadena, California, February 24, 1993.

$$a(f) = \frac{P_{\rm vco}(f)}{P_{\rm uso}(f) + P_{\rm vco}(f)} \tag{18}$$

$$b(f) = \frac{P_{\rm uso}(f)}{P_{\rm uso}(f) + P_{\rm vco}(f)} \tag{19}$$

But the noise processes described by $P_{\rm uso}(f)$ (flicker frequency noise) and $P_{\rm vco}(f)$ (white phase noise) are actually well-known functions:

$$P_{\rm uso}(f) = \frac{A}{f} \tag{20}$$

$$P_{\rm vco}(f) = Bf^2 \tag{21}$$

where A and B are estimated from the data.

Substituting,

$$a(f) = \frac{Bf^2}{(A/f + Bf^2)} \tag{22}$$

$$b(f) = \frac{A/f}{(A/f + Bf^2)} \tag{23}$$

These are the final weighting functions that will be used for combining. Note that in the limit as f approaches zero, $a(f) = 1$ and $b(f) = 0$, while as f gets very large, $a(f) = 0$ and $b(f) = 1$. This is consistent with the idea of selecting coherent data at low frequencies and noncoherent data at high frequencies.

Returning to the analysis, the power spectral density of the USO and VCO velocity residuals, along with the theoretical expectation derived by Kursinski, can be seen in Fig. 11. In order to arrive at these plots, both spectral densities were converted to Doppler velocity spectral density using Eqs. (4) and (5). For the most part, these spectra follow the theoretical asymptotes for their respective noise processes, as in Eqs. (20) and (21). One important exception, however, is the deviation from f^2 at very low frequencies in the VCO data. Potentially this represents the gravity harmonics of Neptune now emerging above the lower f^2 noise floor; however, it also could represent a frequency instability, either in the feedthrough of the transponder mode switch or from some processing error in deriving the synthesized coherent data.

There are three ways of deriving A and B from the data. The first is by linear least-squares fitting the Fourier noise components by the desired modeling function (i.e., $1/f$ or f^2). The second is by computing the Allan variance of the residual frequency time series and using the transformation formulas provided by Barnes et al. [9] for converting to the amplitude of a noise process. The third is by collapsing A and B into a single parameter, A/B, and adjusting it to minimize the combined noise power. Of the three, the second and third methods provided the most consistent results. The first method tended to overestimate the USO noise and underestimate the VCO noise, resulting in an A/B that was twice as large as the other methods. However, the estimates of the first method were chosen for the combining because they produce weighting functions that suppress more of the unwanted USO noise. These are

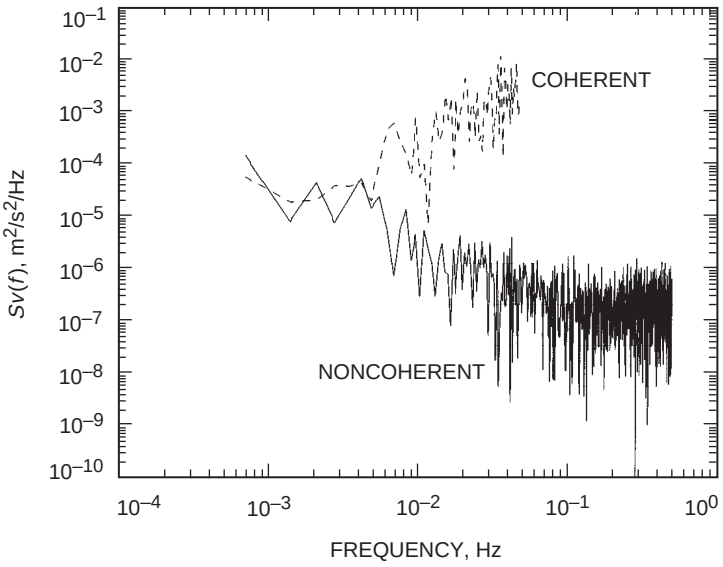

Fig. 11. The velocity spectral density of noncoherent and synthesized coherent downlink (compare with Fig. 2).

$$A = 8.76 \times 10^{-25}$$

$$B = 2.09 \times 10^{-17}\ \mathrm{Hz}^{-3}$$

Figure 12 shows the weighting functions derived from these parameters on both a linear and a log scale. Note that the cross-over frequency (about 3 mHz) agrees remarkably well with Kursinski's prediction in Fig. 2. Figure 13 shows the combined power spectrum, which has the characteristics of the VCO spectrum below 3 mHz and the USO spectrum above 3 mHz.

Finally, Fig. 14 shows the combined coherent and noncoherent data after being referenced to a noncoherent downlink frequency time series (i.e., one-way Doppler). Some idea of the overall improvement can be obtained by comparing this plot with the original noncoherent Doppler data in Fig. 10. In accordance with how the weighting functions select the data, the DC bias and long-term fluctuations (low frequency) of the original USO data have been reduced by the VCO contribution, while the relatively low-noise short-term fluctuations of the USO remain unmodified.

IV. Evaluation of Combined Residuals

There are several ways to determine whether the combined residuals have improved upon the original USO data. The first and simplest is by comparing the standard deviation of the two frequency time series. Indeed, the σ of the combined residuals is 10 percent less than that of the USO residual alone. Unfortunately, the presence of a broad spectrum of noise tends to overshadow the gain that has been achieved at only a subset of frequencies. In addition, the true noise reduction will be masked by the gravity harmonic signature, which prevents the standard deviation from dropping below a certain level.

A second approach is to compute the Allan deviation $\sigma\ (\Delta f/F)$ of the two time series, as shown in Fig. 15. Here it is seen that the long-term frequency instability of the combined residuals is smaller than that of the USO residuals by a factor of 2 over certain time scales (300 to 700 s). While this method allows for an improved frequency selective comparison, the presence of a gravity signature also will tend to limit the estimation of noise reduction.

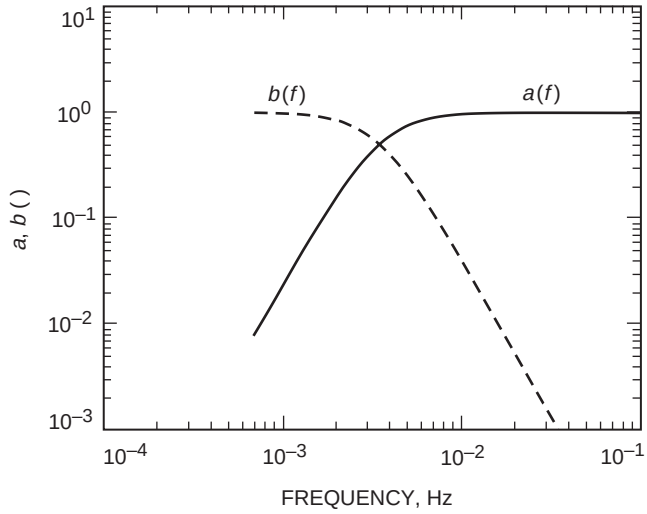

Fig. 12. Fourier combining functions *a*(*f*) and *b*(*f*).

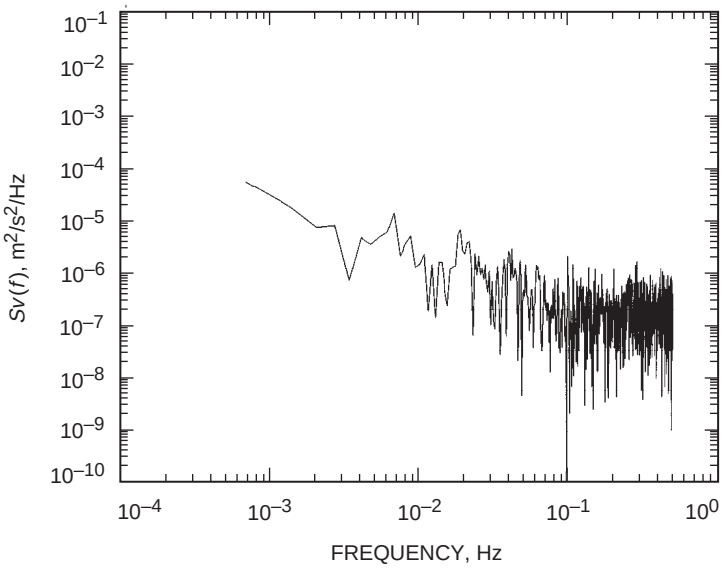

Fig. 13. Velocity spectral density of optimally combined coherent and noncoherent data (compare with Fig. 11).

The third and most effective approach is to perform a gravity field fit to the data. Due to the nonlinear nature of the fit, a small change in the long-term fluctuations of this critical time period can have a large effect on final results. And, in fact, the long-term fluctuations have changed. What appears to be an arbitrary scallop in the USO residuals has been replaced with a smoother, more sinusoidal shape, more amenable to fitting with the gravity signatures from Fig. 3. Interestingly, these same signatures, representing perturbations at about half the uncertainty expected to be derived from the combined data, show a much larger effect than is exhibited in the data itself, suggesting that the original gravity fit was quite good. Although the fact that the noise has been reduced may not change the harmonic estimates, it should reduce their uncertainty when the gravity field is refit with this new data set.

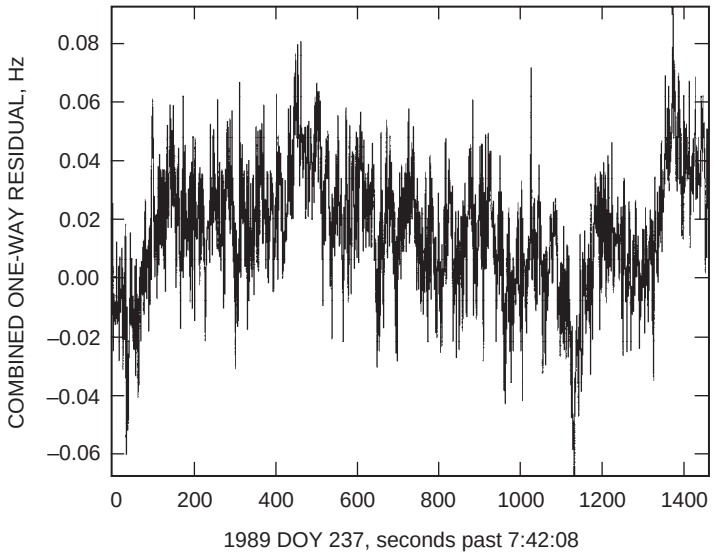

Fig. 14. Optimally combined data converted to noncoherent residuals for comparison with Fig. 10.

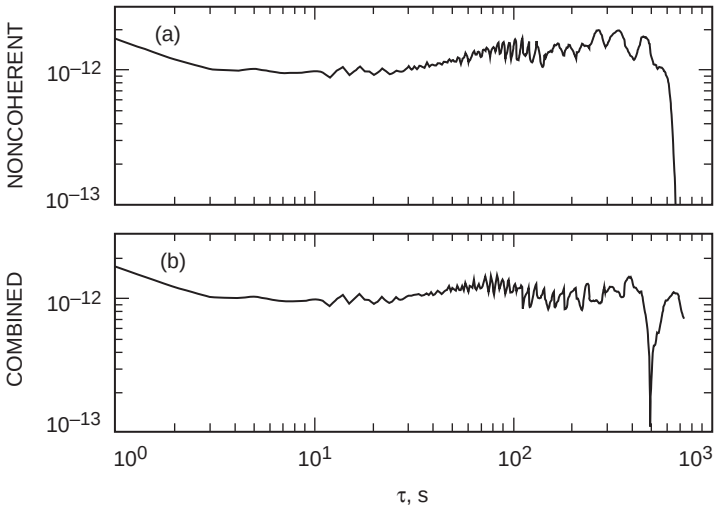

Fig. 15. The Allan deviation $\sigma(\Delta f/F)$ of (a) original noncoherent and (b) improved noncoherent frequency residuals, showing a decrease of noise at large τ.

V. Conclusions

A number of techniques allowing for the extraction and useful application of coherent Doppler when a spacecraft transmits in noncoherent mode have been developed in the course of this work. These include signal-processing techniques for extracting the weak coherent feedthrough side tones, Fourier techniques for optimally combining two data sets with different noise characteristics, and analysis techniques for predicting the performance of the final result.

With the Neptune ingress data set, a real demonstration of the above techniques has resulted in a 50 percent improvement in long-term Allan deviation σ over the original noncoherent Doppler data. The improved data set will be incorporated into a refined Neptune gravity fit and is expected to reduce the uncertainty in the J2 and J4 gravity harmonics by a similar degree.

Alternatively, the same techniques can be used to extract noncoherent Doppler from a coherent downlink. The consequence of having two simultaneous measurements of spacecraft Doppler available for radio science has yet to be fully realized; however, some possible applications include (1) improvement in polar gravity field measurements with Mars Global Surveyor over the 5-min noncoherent segment at every egress, (2) optimal combining of Cassini's coherent/noncoherent Ka-band (32-GHz) downlinks to improve the short-term coherent noise, and (3) use of a synthesized noncoherent downlink to provide measurements of gravitational redshift when a spacecraft is in coherent mode.

Acknowledgments

From concept to completion, the work in this article spans almost 10 years, involving substantial input from many people. The authors thank George Lewis, Bob Jacobson, Miles Standish, and Rick Sunseri for recovering the original Voyager–Neptune trajectory fit; Gene Goltz and K.J. Lee for ongoing support in computing Doppler residuals; Bill Folkner for retaining a Voyager-era orbit determination program (ODP) on his VAX; John Armstrong for his many helpful suggestions throughout the project; and John Anderson, Eunice Lau, and Jim Campbell for guidance and feedback on gravity field applications. We especially thank David Morabito for providing radio science software that produced the necessary VCO and Doppler model time series.

References

[1] G. L. Tyler, D. N. Sweetnam, J. D. Anderson, S. E. Borutzki, J. K. Campbell, V. R. Eshleman, D. L. Gresh, E. M. Gurrola, D. P. Hinson, N. Kawashima, E. R. Kursinski, G. S. Levy, G. F. Lindal, J. R. Lyons, E. A. Marouf, P. A. Rosen, R. A. Simpson, and G. E. Wood, "Voyager Radio Science Observations of Neptune and Triton," *Science*, vol. 246, pp. 1466–1473, 1989.

[2] J. D. Anderson, E. L. Lau, W. L. Sjogren, G. Schubert, and W. B. Moore, "Europa's Differentiated Internal Structure: Inferences From Two Galileo Encounters," *Science*, vol. 276, pp. 1236–1239, May 23, 1997.

[3] J. D. Anderson, in *Experimental Gravitation*, B. Bertotti, ed., New York: Academic Press, pp. 163–199, 1974.

[4] T. A. Rebold and J. F. Weese, "Parkes Radio Science System Design and Testing for Voyager Neptune Encounter," *The Telecommunications and Data Acquisition Progress Report 42-99, July–September 1989*, Jet Propulsion Laboratory, Pasadena, California, pp. 189–205, November 15, 1989.

[5] N. C. Ham, T. A. Rebold, and J. F. Weese, "DSN Radio Science System Design and Testing for Voyager Neptune Encounter," *The Telecommunications and Data Acquisition Progress Report 42-97, January–March 1989*, Jet Propulsion Laboratory, Pasadena, California, pp. 252–284, May 15, 1989.

[6] W. H. Press, B. P. Flannery, S. A. Teukolsky, and W. T. Vetterling, *Numerical Recipes*, New York: Cambridge University Press, pp. 521–528, 1990.

[7] R. A. Jacobson, J. E. Riedel, and A. H. Taylor, "The Orbits of Triton and Nereid From Spacecraft and Earth-Based Observations," *Astron. Astrophysics*, vol. 247, pp. 565–575, 1991.

[8] D. D. Morabito and S. W. Asmar, "Radio-Science Performance Analysis Software," *The Telecommunications and Data Acquisition Progress Report 42-120, October–December 1994*, Jet Propulsion Laboratory, Pasadena, California, pp. 121–152, February 15, 1995.
http://tda.jpl.nasa.gov/tda/progress_report/42-120/120B.pdf

[9] J. A. Barnes, A. R. Chi, L. S. Cutler, D. J. Healey, D. B. Leeson, T. E. McGunigal, J. A. Mullen, W. L. Smith, R. Sydnor, R. F. C. Vessot, and G. M. R. Winkler, *Characterization of Frequency Stability*, NBS Technical Note 394 (Catalog no. C13.46:394), U.S. Government Printing Office, October 1970.